Spectroscopic properties of heavily Ho^{3+}-doped barium yttrium fluoride crystals*

Ji En-Cai(吉恩才)[a], Liu Qiang(柳 强)[a]†, Nie Ming-Ming(聂明明)[a], Luo Hui (罗 辉)[b], Hu Yu-Xi(胡玉熙)[b], Guan Zhou-Guo(官周国)[b], and Gong Ma-Li(巩马理)[a]

[a] *State Key Laboratory of Precision Measurement Technology and Instruments, Center for Photonics and Electronics, Department of Precision Instrument, Tsinghua University, Beijing* 100084, *China*

[b] *Southwest Technical Institute of Physics, Chengdu* 610061, *China*

(Received 30 May 2015; revised manuscript received 7 July 2015; published online 3 August 2015)

The 30 at.% Ho: BaY_2F_8 crystals were grown by the Czochralski method, and their spectroscopic properties are analyzed systematically by standard Judd–Ofelt theory. The Judd–Ofelt intensity parameters are estimated to be $\Omega_2 = 6.74\times10^{-20}$ cm^2, $\Omega_4 = 1.20\times10^{-20}$ cm^2, and $\Omega_6 = 0.66\times10^{-20}$ cm^2, and the fluorescence branching ratios and radiative lifetimes for a series of excited state manifolds are also determined. The emission cross sections with our measured infrared luminescence spectra, especially important for 4.1 μm, are calculated to be about 4.37×10^{-21} cm^2. The crystal quality is preliminarily tested through a mid-infrared laser emission experiment.

Keywords: Ho:BYF crystal, Judd–Ofelt theory, mid-infrared laser

PACS: 42.70.Hj, 42. 55.Rz **DOI:** 10.1088/1674-1056/24/9/094216

1. Introduction

The 3–5 micron mid-infrared lasers are of significance for applications due to their many good characteristics, such as high transmittance through atmosphere, low background noise and special absorption spectrum of most important gas molecules.[1–3] Currently, with the nonlinear frequency conversion technology, high energy or high average power mid-infrared lasers can be obtained.[4–6] Nonetheless, the overall design principle and mechanical structure, at least two-stage scheme, still seem to be a little complex. Meanwhile, the quantum cascade laser (QCL) based on intersubband transitions within a multiple-quantum-well structure can obtain a wide tuning range of 3–25 μm.[7] However, it is difficult to further improve the output power and efficiency in a short term. With the development of material science and engineering, some new fabricated laser crystals are found to have low enough multi-phonon decay rates, which are beneficial to long wavelength emission, such as rare earth (RE) or transition metal (TM) ions doped hosts.[8–10] In consequence, utilizing the direct pumping scheme of only single-stage oscillator will be increasingly significant to obtain mid-infrared laser.

Among the RE-ion doped crystals, holmium-doped barium yttrium fluoride (Ho^{3+}:BaY_2F_8, simplified as Ho: BYF) has been proven to emit 3.9 μm pulsed laser efficiently.[11,12] In 2011, Tsuboi *et al.*[13] first investigated the ultraviolet, visible, and near IR luminescence spectra (<2.4 μm) of Ho: BYF at room temperature and by cryogenic cooling way separately. To date, no one has calculated the detailed spectroscopic parameters of Ho: BYF completely with the Judd–Ofelt (J–O) theory,[14,15] which are vital to the dynamics analysis of Ho: BYF laser. And Stutz *et al.*'s model of 3.9 μm Ho: BYF laser[16] still has some flaws. More importantly, the parameters are crucial for designing the way to co-dope sensitized ion into Ho: BYF to further enhance the mid-infrared excitation efficiency.

In this work, we will analyze in detail the spectroscopic properties of heavily-doped Ho: BYF crystal, grown by Czochralski (CZ) method. With the calculations of three phenomenological J–O intensity parameters Ω_i ($i = 2,4,6$), we can further obtain the transition parameters, including spontaneous emission probabilities, fluorescence branching ratios and radiative lifetimes, etc. Additionally, the emission cross sections can be calculated with two different methods, based on absorption spectra or luminescence spectra.

2. Experimental techniques

For growing the Ho: BYF single crystal, the spectrophotometric grade oxide reagents of Ho_2O_3, Y_2O_3, and $BaCO_3$ were taken as the raw materials, and the molar ratio was 0.3:0.7:1. The oxide reagents were first dissolved by the reaction of halogenation with hydrochloric acid, and Ho: BYF with monoclinic structure was synthesized at a high temperature of 800 °C by hydrothermal and co-precipitation methods. Single crystal Ho: BYF was grown by CZ method in a

*Project supported by the National Natural Science Foundation of China (Grant No. 61275146), the Research Fund for the Doctoral Program of Higher Education of China (Grant No. 20120002110066), and the Special Program of the Co-construction with Beijing Municipal Government of China (Grant No. 20121000302).

†Corresponding author. E-mail: qiangliu@mail.tsinghua.edu.cn

© 2015 Chinese Physical Society and IOP Publishing Ltd

platinum crucible and the chamber was first vacuumized to about 0.003 Pa. The crucible was maintained at a temperature of 800 °C with graphite resistance heating system for 10 h, then, high-purity argon gas (> 99.999%) and volume fraction of 5% hydrogen fluoride gas were flowed into the furnace to further eliminate the water and oxygen. After seeding in the direction *b*, [010], the crystal rotation and pulling rates were fixed at 5 rpm and 1 mm/h, respectively, and the pressure was increased to 0.02 MPa. Finally, we obtained a transparent Ho: BYF crystal with holmium-doped concentration of 30 at.%, as shown in Fig. 1, and it has adequate quality for the x-ray diffraction analysis.[17] The size of manufactured Ho: BYF crystal for spectrum measurement was 15 mm × 7.5 mm × 2 mm with a rectangular section, and two end faces were uncoated.

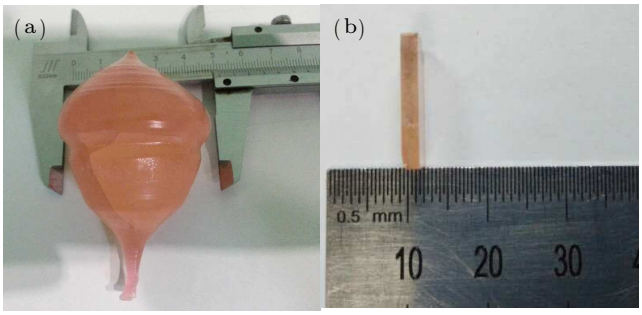


Fig. 1. (color online) Picture of $BaY_{1.4}$ $Ho_{0.6}F_8$ crystal. (a) Picture of monocrystal Ho: BYF ingot (pale orange) with CZ method under the fluorescent lamp irradiation, (b) picture of cuboid Ho: BYF crystal (pale yellow) after being processed under the natural light.

The absorption spectrum of Ho: BYF in a wavelength range of 200–2500 nm was measured with a UV–Vis–NIR spectrophotometer (Cary 5000, UV1009M292, Agilent Technologies), whose spectral resolution is 0.02 nm in the ultraviolet (UV) range and about 0.5 nm in the near infrared (NIR) range. The infrared luminescence spectrum of Ho: BYF, pumped by a CW tunable Ti: sapphire laser (Mira 900-D, Coherent), was detected with a liquid-nitrogen cooled InSb photo-diode (Dmni-λ3015, Zolix) and a lock-in amplifier (Model420, Scttec).

The host material of Ho: BYF is monoclinic biaxial BaY_2F_8 crystal, whose crystallographic axes, principal axes and optic axes are shown in Fig. 2(a). Apparently, only the *b* crystallographic axis coincides with the *y* principal axis, and the angle between two other crystallographic axes is about 99.7°. Trivalent holmium ion (Ho^{3+}) is merely a little smaller in size than trivalent yttrium ion (Y^{3+}), but quite different from barium ion (Ba^{2+}). So Ho^{3+} will substitute for Y^{3+} more easily than Ba^{2+} in BaY_2F_8, and Ho: BYF crystal has nearly the monoclinic structure.[18] The phonon energy of BaY_2F_8 is about 420 cm^{-1} according to the vibrational spectra measured by Kaminskii[19] or Guilbert,[20] and is almost the lowest among fluorides. Figure 2(b) shows the cut direction of our samples, so the laser propagates through the *b* axis.

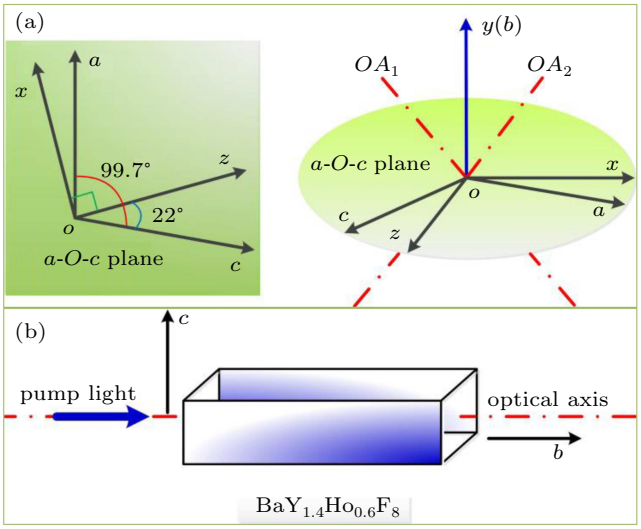


Fig. 2. (color online) Schematic diagram of Ho: BYF crystal sructure. (a) crystallographic axes (a,b,c), principal axes (x,y,z) and optic axes (OA_1, OA_2) in BaY_2F_8; (b) crystallographic axes (b, c) in our processed Ho: BYF crystal.

3. Results and discussion

3.1. Analyses of absorption spectrum

The transmittance spectra of Ho: BYF at room temperature of 298 K are shown in Fig. 3, including UV range of 200–385 nm in Fig. 3(a), visible range of 385–850 nm in Fig. 3(b), and near-infrared range of 850–3200 nm in Fig. 3(c). Apparently, there is a series of characteristic absorption peaks in these figures, and some of them are listed in Table 1 with their corresponding transition processes.

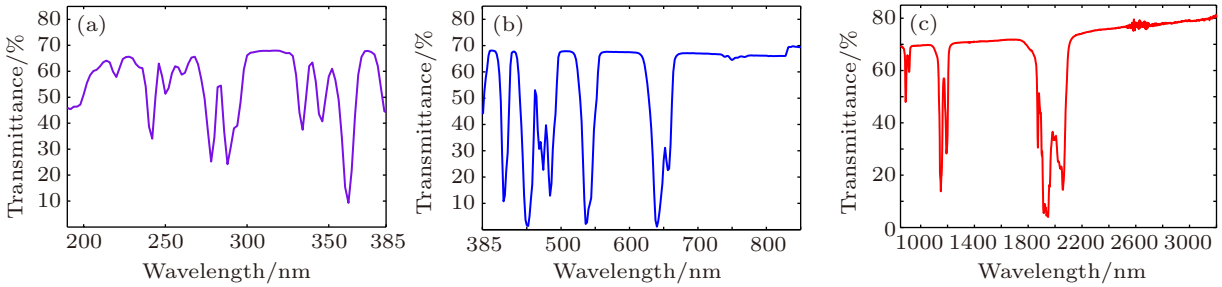


Fig. 3. Measured transmittance spectra of 30 at.% Ho: BYF at room temperature. (a) UV light band, (b) visible light band, (c) near IR light band.

Table 1. Values of wavelength of absorption peak (λ_{ap}) and the corresponding transitions from measured spectra in Fig. 3.

Range	λ_{ap}/nm	Transitions
UV light	362	$^5I_8 \rightarrow {}^3H_6$
	384	$^5I_8 \rightarrow {}^5G_4 + {}^3K_7$
Visible light	416	$^5I_8 \rightarrow {}^5G_5$
	452	$^5I_8 \rightarrow {}^5G_6 + {}^5F_1$
	484	$^5I_8 \rightarrow {}^5F_2 + {}^3K_8$
	536	$^5I_8 \rightarrow {}^5F_4 + {}^5S_2$
	640	$^5I_8 \rightarrow {}^5F_5$
	748	$^5I_8 \rightarrow {}^5I_4$
NIR light	888	$^5I_8 \rightarrow {}^5I_5$
	1150	$^5I_8 \rightarrow {}^5I_6$
	1948	$^5I_8 \rightarrow {}^5I_7$

The optical density spectrum is shown in Fig. 4, which can be easily calculated with transmittance spectra from the following expression:

$$OD(\lambda) = -\lg[T(\lambda)], \tag{1}$$

where $OD(\lambda)$ is the optical density varying with wavelength λ, and $T(\lambda)$ is the transmittance through Ho: BYF.

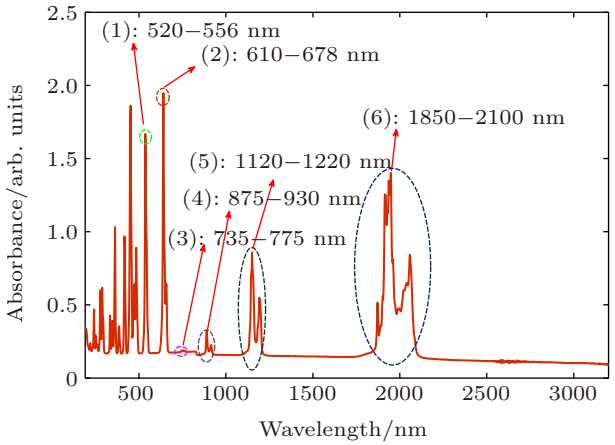


Fig. 4. Optical density spectrum of Ho: BYF with six chosen absorption bands.

We choose six important absorption bands from Table 1 based on the absorption spectrum, and depict the seven lower energy level distributions in Fig. 5.

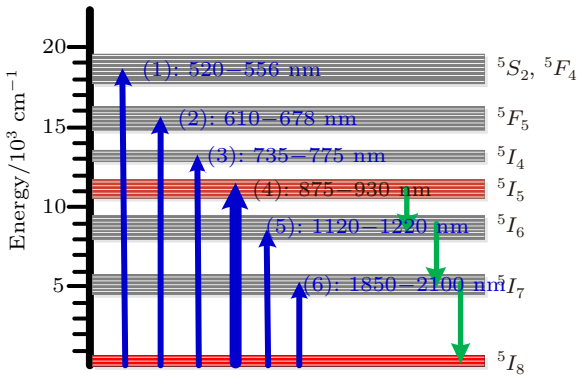


Fig. 5. (color online) Sketch map of the energy level structure and the absorption transitions of Ho^{3+}.

Only in consideration of the electric dipole (ED) transitions,[21–23] can the spectral line strengths $S_{JJ'}$ and the oscillator strengths $P_{JJ'}$ of six chosen transitions above be obtained with Judd–Ofelt theory from the following expression:

$$\begin{cases} S_{JJ'} = \dfrac{3hc(2J+1)}{8\pi^3 E^2 N_J l_c \lambda_a \chi \log(e)} \displaystyle\int OD(\lambda)\,\mathrm{d}\lambda, \\ P_{JJ'} = \dfrac{8\pi^2 mc\chi}{3h\lambda_a(2J+1)} S_{JJ'}, \end{cases} \tag{2}$$

where $J(J')$ is the total angular momentum of ground state (excited state), h the Planck's constant, c the light speed in vacuum, λ_a the average absorption wavelength of transition, l_c the length of Ho: BYF, E the electron charge, n the refractive index of Ho: BYF corresponding to λ_a, m the electron mass, and $\chi = (n^2+2)^2/9n$ the field correction factor.[22] For Ho: BYF, the value of J is 8, and the length l_c is 2 mm.

In addition, the relations among single-pass absorption coefficient $\alpha(\lambda)$, absorption cross section $\sigma_a(\lambda)$ and $OD(\lambda)$ can be easily derived as follows:

$$\begin{cases} \alpha(\lambda) = \dfrac{OD(\lambda)}{l_c \log(e)}, \\ \sigma_a(\lambda) = \dfrac{\alpha(\lambda)}{N_J}, \end{cases} \tag{3}$$

where e is the base of natural logarithm. Obviously, when $OD(\lambda)$ and l_c are given, $\alpha(\lambda)$ and $\sigma_a(\lambda)$ can be easily obtained, meanwhile, the refractive index $n(\lambda)$ is needed to further figure out $S_{JJ'}$ and $P_{JJ'}$.

One-term Sellmeier dispersion equation of BaY_2F_8 can be referred from Ref. [24] by Weber in 1995 as follows:

$$\frac{1}{n^2(\lambda)-1} = -\frac{A}{\lambda^2} + B. \tag{4}$$

The calculated refractive indices are only mean values, and the coefficients $A = 0.0053$ and $B = 0.7707$.

Considering the refractive indices at wavelength of 589.3 nm are 1.5235, 1.5356, and 1.5145, respectively for (x, y, z) axes,[24] we calculate the angle $\beta = 41.07°$ between optic axes (OA_1 or OA_2 as shown in Fig. 2(a)) and y-axis from the following expression:

$$\tan\beta = \frac{n_y}{n_z}\sqrt{\frac{n_x^2 - n_z^2}{n_y^2 - n_x^2}}. \tag{5}$$

Apparently, the BYF crystal is biaxial positive as n_x is closer to n_y in magnitude than to n_z, namely $\beta < 45°$. For the holmium doped BYF crystal, we assume that the dispersion equation is the same as that of BYF crystal.

In general, birefringence will appear when light passes through a biaxial crystal along neither of its optic axes, and the refractive indices are different for two kinds of extraordinary light. However, we neglect the walk-off effect to simplify

the calculation process, and take the mean refractive index of principal axes in Eq. (4) as the value of undetermined $n(\lambda)$ in Eqs. (2) and (3).

Substituting the values of refractive index and the optical density into Eqs. (2) and (3), we obtain the values of $S_{JJ'}$ and $P_{JJ'}$ as listed in Table 2, and calculate the values of $\alpha(\lambda)$ and $\sigma_a(\lambda)$ of six typical absorption peak wavelengths, which are listed in Table 3.

Table 2. Calculated results of spectral line strengths $S_{JJ'}$ and oscillator strengths $P_{JJ'}$.

Transitions	$\lambda_a/10^{-7}$ cm	n/λ_a	$\int OD(\lambda)\,d\lambda/10^{-7}$ cm	$S_{JJ'}/10^{-21}$ cm^2	$P_{JJ'}/10^{-7}$
$^5I_8 \rightarrow {}^5F_4+{}^5S_2$	538	1.5261	22.85	7.20	11.65
$^5I_8 \rightarrow {}^5F_5$	649	1.5228	34.34	8.99	12.04
$^5I_8 \rightarrow {}^5I_4$	755	1.5210	7.68	1.73	1.99
$^5I_8 \rightarrow {}^5I_5$	903	1.5194	11.42	2.15	2.07
$^5I_8 \rightarrow {}^5I_6$	1170	1.5179	37.93	5.53	4.09
$^5I_8 \rightarrow {}^5I_7$	1975	1.5165	153.49	13.27	5.81

Table 3. Calculated results of $\alpha(\lambda)$ and $\sigma_a(\lambda)$ for six typical wavelengths of absorption peaks.

$\lambda_{ap}/10^{-7}$ cm	536	640	748	888	1150	1948
$\alpha(\lambda)/\text{cm}^{-1}$	8.34	9.74	0.94	1.60	4.30	7.01
$\sigma_a(\lambda)/10^{-21}$ cm^2	2.18	2.54	0.25	0.42	1.12	1.83

3.2. Calculation for Ω_i

The relationship between the ED line strengths $S_{JJ'}$ and J–O intensity parameters Ω_i can be expressed as

$$S_{JJ'} = \sum_{i=2,4,6} \Omega_i \left| \langle 4f^n \psi J | \left| U^{(i)} \right| | 4f^n \psi' J' \rangle \right|^2, \tag{6}$$

where $U^{(i)}$ is the irreducible tensor of ED operator, $\langle 4f^n \psi J||U^{(i)}||4f^n \psi' J'\rangle$ is usually written as $|U^{(i)}|^2$ which is doubly reduced matrix element.[21] In order to calculate Ω_i, the value of $|U^{(i)}|^2$ is needed at least with three different transition processes. Considering the fact that the host material has little effect on the value of $|U^{(i)}|^2$, we take this value as the value of Ho^{3+} in aqueous solution (aq), or Ho^{3+} in LaF_3 crystal in Refs. [25] and [26], and list $|U^{(i)}|^2$ of six different transitions[26] in Table 4.

Table 4. Doubly reduced matrix element for Ho^{3+}.

Transition processes	(1)	(2)	(3)	(4)	(5)	(6)
$\|U^{(2)}\|^2$	0	0	0	0	0.0083	0.0249
$\|U^{(4)}\|^2$	0.2402	0.4277	0	0.099	0.0383	0.1344
$\|U^{(6)}\|^2$	0.7079	0.5686	0.0077	0.0936	0.6918	1.5217

Apparently, with different transitions, an equation set is obtained in the form of matrix as follows:

$$\boldsymbol{M}\boldsymbol{\Omega} = \boldsymbol{S}, \tag{7}$$

where $\boldsymbol{M}$ is the matrix of the reduced matrix elements, in which each row vector is corresponding to one kind of transition, $\boldsymbol{S}$ the matrix of ED line strengths, and $\boldsymbol{\Omega}$ the matrix of J–O intensity parameters.

According to the known values in Tables 2 and 4, we obtain the matrixes $\boldsymbol{S}$ and $\boldsymbol{M}$ as follows:

$$\boldsymbol{S} = \begin{bmatrix} 7.20 \\ 8.99 \\ 1.73 \\ 2.15 \\ 5.53 \\ 13.27 \end{bmatrix} \times 10^{-21}\ \text{cm}^2,$$

$$\boldsymbol{M} = \begin{bmatrix} 0 & 0.2402 & 0.7079 \\ 0 & 0.4277 & 0.5686 \\ 0 & 0 & 0.0077 \\ 0 & 0.0099 & 0.0936 \\ 0.0083 & 0.0383 & 0.6918 \\ 0.0249 & 0.1344 & 1.5217 \end{bmatrix}. \tag{8}$$

The number of rows of matrix $\boldsymbol{M}$ is always larger than that of matrix $\boldsymbol{\Omega}$, optimization method is necessary to find the approximate solution. Herein we use the least square method (LSM) and the optimal solution $\boldsymbol{\Omega}_{op}$ is obtained as

$$\boldsymbol{\Omega}_{op} = \left(\boldsymbol{M}^T\boldsymbol{M}\right)^{-1}\boldsymbol{M}^T\boldsymbol{S}. \tag{9}$$

Meanwhile, to calculate the fitting error, we substitute the oscillator strengths in Eq. (2) and spectral line strengths in Eq. (7) with the above optimal solution $\boldsymbol{\Omega}_{op}$, namely they are expressed as follows:

$$\begin{cases} \boldsymbol{S}_{exp} = \boldsymbol{S}, \boldsymbol{P}_{exp} = \dfrac{8\pi^2 mc\chi}{3h\lambda_a(2J+1)}\boldsymbol{S}_{exp}, \\ \boldsymbol{S}_{cal} = \boldsymbol{M}\boldsymbol{\Omega}_{op}, \boldsymbol{P}_{cal} = \dfrac{8\pi^2 mc\chi}{3h\lambda(2J+1)}\boldsymbol{S}_{cal}, \end{cases} \tag{10}$$

where $\boldsymbol{S}_{exp}$ and $\boldsymbol{P}_{exp}$ are matrixes of spectral line strengths and oscillator strengths respectively based on experiment, while $\boldsymbol{S}_{cal}$ and $\boldsymbol{P}_{cal}$ are counterparts based on the optimal solution.

The errors δ_S and δ_P, corresponding to the calculated line strengths and the oscillator strengths respectively, are then shown below in the form of root-mean-square error (RMSE).

$$\delta_S = \sqrt{\frac{\text{sum}\left[\left(\boldsymbol{S}_{cal} - \boldsymbol{S}_{exp}\right)^2\right]}{3}},$$

$$\delta_P = \sqrt{\frac{\text{sum}\left[\left(P_{\text{cal}} - P_{\text{exp}}\right)^2\right]}{3}}. \tag{11}$$

Finally, we obtain the results of Ω_{op}, δ_S, and δ_P as follows:

$$\begin{cases} \Omega_{\text{op}} = \begin{bmatrix} \Omega_2 \\ \Omega_4 \\ \Omega_6 \end{bmatrix} = \begin{bmatrix} 6.74 \\ 1.20 \\ 0.66 \end{bmatrix} \times 10^{-20}\ \text{cm}^2, \\ \delta_S = 1.29 \times 10^{-21}\ \text{cm}^2,\ \ \delta_P = 1.40 \times 10^{-7}. \end{cases}$$

The J–O intensity parameters of Ho^{3+} single-doped crystal for many kinds of glass hosts or fiber hosts have been reported. Here, we enumerate some of them in Table 5,[27–32] and compare them with those of the present BYF-based crystal. It can be easily found from Table 5 that the Ω_2 parameter of Ho: BYF is much larger than those of other fluoride crystals and similar to those of $ZnCl_2$-based chloride crystal and Sc_2O_3-based oxide ceramic, indicating that the covalency of chemical bond between holmium and fluoride ions is relatively strong;[33] the Ω_6 parameter of Ho: BYF is very small, so the spontaneous emission probability should be small and the radiative lifetime may be large;[34] the Ω_4/Ω_6 value of Ho: BYF is a little smaller than those of $ZnCl_2$, KYF or SC_2O_3-based crystals, which reflects that the fifth odd term of crystal field has a more important influence on the $4f^n$ transition than the third odd term.[35]

Table 5. J–O intensity parameters of several Ho^{3+} single doped crystals.

Host materials	CaF_2[27]	$ZnCl_2$[28]	YAG[29]	KYF[30]	Sc_2O_3[31]	YLF[32]	BYF*
Concentration	1%	3%	0.5%	0.5%	0.2%	1%	30%
$\Omega_2/10^{-20}\ \text{cm}^2$	0.018	7.07	0.101	0.48	6.01	1.14	6.74
$\Omega_4/10^{-20}\ \text{cm}^2$	0.57	2.43	2.086	2.91	1.99	0.79	1.20
$\Omega_6/10^{-20}\ \text{cm}^2$	0.587	0.77	1.724	0.73	0.49	1.33	0.66
Ω_4/Ω_6	0.971	3.156	1.210	3.986	4.061	0.594	1.818

*Ho: BYF, in this work.

3.3. Calculation for transition parameters

With the J–O intensity parameters, we calculate the radiation transitional parameters,[23] such as spontaneous emission probability $A_{JJ'}$, fluorescence branching ratio $\beta_{JJ'}$ and radiative lifetime τ_J from the following expressions:

$$\begin{cases} A_{JJ'} = \dfrac{64\pi^4 e^2 n \left(n^2+2\right)^2}{27h\lambda^3 (2J+1)} \\ \qquad \times \sum\limits_{i=2,4,6} \Omega_i \left|\langle 4f^n \psi J| \left|U^{(i)}\right| |4f^n \psi' J'\rangle\right|^2, \\ \beta_{JJ'} = \dfrac{A_{JJ'}}{\sum\limits_{J'} A_{JJ'}}, \\ \tau_J = \dfrac{1}{\sum\limits_{J'} A_{JJ'}}. \end{cases} \tag{12}$$

The emission transition parameters are calculated with Eqs. (5) and (12), and the results are listed in Table 6 for emission probability $A_{JJ'}$, fluorescence branching ratio $\beta_{JJ'}$, and in Table 7 for radiative lifetime τ_J.

The effect of magnetic dipole (MD) is not considered in this work, so the spurious exceptions can be expected in Tables 6 and 7 compared with the results in Ref. [16], such as the radiative lifetime of $^5I_7$ (about 42 ms, larger than about 17 ms in Ref. [16]), and the radiative lifetime of $^5I_6$ (about 18.4 ms, also larger than about 5.4 ms in Ref. [16]), but the fluorescence branching ratios β_{56}, β_{57}, β_{58} (0.057, 0.563, 0.380) are similar to those (0.0674, 0.5381, 0.3944) of Ho: YLF crystal in Ref. [24]. Apparently, the calculated radiative lifetimes are a little larger than the values reported in Ref. [16]. It is because, on the one hand, the Ho^{3+} concentration is different from those of samples in Ref. [24], on the other hand, our standard Judd–Ofelt model neglects the effects of magnetic dipole.

If we only take account of the contribution of MD to emission probability, then equation (11) can be counted as follows:[23]

$$\begin{cases} A_{\text{md}} = \dfrac{64\pi^4 e^2 n^3}{3h\lambda^3 (2J+1)} S_{\text{md}}, \\ S_{\text{md}} = \dfrac{h^2}{16m^2c^2\pi^2} \\ \qquad \times \left|\langle 4f^n \psi J| \left|L+2S\right| |4f^n \psi' J'\rangle\right|^2, \end{cases} \tag{13}$$

where A_{md} is the contribution of MD to emission probability, S_{md} is the MD transition spectral line strength, L is the angular momentum operator, and S is the spin operator.

In the LS coupling scheme, the contributions of MD to emission probability of transitions $^5I_7 \rightarrow {}^5I_8$, $^5I_6 \rightarrow {}^5I_7$, $^5I_5 \rightarrow {}^5I_6$, $^5I_4 \rightarrow {}^5I_5$, $^5F_4 \rightarrow {}^5F_5$ are 21.61 s^{-1}, 11.57 s^{-1}, 5.40 s^{-1}, 2.46 s^{-1}, and 7.32 s^{-1}, respectively. Obviously, the radiative lifetimes and the fluorescence branching ratios will change accordingly, and the adjusted radiative lifetimes of $^5I_7$, $^5I_6$, $^5I_5$, $^5I_4$ are 22.03 ms, 15.15 ms, 25.32 ms, and 50.63 ms, respectively. Assuming that the observed lifetimes are the same as those in Ref. [16], namely the radiative lifetimes of $^5I_7$, $^5I_6$, $^5I_5$ are 17 ms, 5.4 ms, and 0.052 ms, respectively, the non-radiative lifetimes of $^5I_7$, $^5I_6$, $^5I_5$ can be easily calculated to be 74.46 ms, 8.39 ms, and 0.0521 ms, respectively, based on the following equation:

$$\tau_{\text{nr}} = \frac{1}{W_{\text{nr}}} = \frac{1}{1/\tau_{\text{m}} - 1/\tau_{\text{r}}}, \tag{14}$$

where τ_{nr} is the non-radiative lifetime, W_{nr} is the non-radiative relaxation rate, τ_{m} is the observed radiative lifetime, and τ_{r} is the calculated radiative lifetime.

Table 6. Calculated results of emssion transional parameters ($A_{JJ'}$ and $\beta_{JJ'}$).

Transitions	$\Delta E/\mathrm{cm}^{-1}$	λ_0/nm	$n(\lambda_0)$	$\lvert U^{(i)}\rvert^2$			$A_{JJ'}/\mathrm{s}^{-1}$	$\beta_{JJ'}$
				$i=2$	$i=4$	$i=6$		
$^5I_7 \rightarrow {}^5I_8$	5133	1948	1.5165	0.0249	0.1344	1.5217	23.78	1
$^5I_6 \rightarrow {}^5I_7$	3562	2807	1.5161	0.0319	0.1336	0.9308	5.89	0.108
$^5I_6 \rightarrow {}^5I_8$	8696	1150	1.5180	0.0083	0.0383	0.6918	48.56	0.892
$^5I_5 \rightarrow {}^5I_6$	2566	3898	1.5160	0.0438	0.1705	0.5729	1.95	0.057
$^5I_5 \rightarrow {}^5I_7$	6128	1632	1.5169	0.0027	0.0226	0.8887	19.19	0.563
$^5I_5 \rightarrow {}^5I_8$	11261	888	1.5195	0	0.0099	0.0936	13.96	0.380
$^5I_4 \rightarrow {}^5I_5$	2108	4745	1.5159	0.0312	0.1237	0.9099	1.18	0.068
$^5I_4 \rightarrow {}^5I_6$	4673	2140	1.5164	0.0022	0.0281	0.6640	6.55	0.379
$^5I_4 \rightarrow {}^5I_7$	8236	1214	1.5178	0	0.0033	0.1568	7.94	0.459
$^5I_4 \rightarrow {}^5I_8$	13369	748	1.5211	0	0	0.0077	1.62	0.094
$^5F_5 \rightarrow {}^5I_4$	2256	4433	1.5159	0.0001	0.0059	0.0040	0.02	0
$^5F_5 \rightarrow {}^5I_5$	4364	2292	1.5163	0.0068	0.0271	0.1649	2.05	0.003
$^5F_5 \rightarrow {}^5I_6$	6929	1443	1.5172	0.0102	0.1213	0.4995	23.90	0.040
$^5F_5 \rightarrow {}^5I_7$	10492	953	1.5190	0.0177	0.3298	0.4342	122.72	0.204
$^5F_5 \rightarrow {}^5I_8$	15625	640	1.5230	0	0.4277	0.5686	453.44	0.753
$^5S_2+{}^5F_4 \rightarrow {}^5F_5$	3032	3299	1.5160	0.1944	0.1033	0.0116	5.27	0.005
$^5S_2+{}^5F_4 \rightarrow {}^5I_4$	5288	1891	1.5166	0.0014	0.0513	0.5382	8.31	0.009
$^5S_2+{}^5F_4 \rightarrow {}^5I_5$	7395	1352	1.5174	0.0018	0.1357	0.5717	29.52	0.031
$^5S_2+{}^5F_4 \rightarrow {}^5I_6$	9961	1004	1.5187	0.0012	0.2786	0.3238	72.87	0.077
$^5S_2+{}^5F_4 \rightarrow {}^5I_7$	13523	740	1.5212	0	0.1988	0.4420	174.74	0.184
$^5S_2+{}^5F_4 \rightarrow {}^5I_8$	18657	536	1.5262	0	0.2402	0.7079	660.44	0.694

Table 7. Calculated results of emssion transional parameter τ_J.

Upper level	$\sum_{J'} A_{JJ'}/\mathrm{s}^{-1}$	τ_J/ms
$^5I_7$	23.78	42.05
$^5I_6$	54.45	18.37
$^5I_5$	34.1	29.33
$^5I_4$	17.29	57.84
$^5F_5$	602.13	1.66
$^5S_2+{}^5F_4$	951.15	1.05

Finally, we further calculate the emission cross section σ_e with the equation of reciprocity relating emission to absorption derived by McCumber[36] and Payne *et al.*,[37] which is given as

$$\sigma_e(\nu_s) = \sigma_a(\nu_s)\frac{Z_l}{Z_u}\exp\left(\frac{E_0 - h\nu_s}{k_B T}\right), \quad (15)$$

where ν_s is the frequency of signal light, Z_l and Z_u are the partition functions of the lower and upper manifolds, respectively, E_0 is the energy difference between the lowest crystal-field level of the upper laser state and the lowest crystal-field level of the lower laser state, k_B is the Boltzmann constant, and the temperature T of the laser crystal is assumed to be room temperature of 298 K. The Z_l/Z_u, and E_0 are very important parameters for the calculation, herein we mainly refer Walsh *et al.*'s paper[23] in which the spectroscopic properties of Ho: YLF was analyzed.

With the experimental value of σ_a in Table 3, we obtain σ_e for several chosen transitions as shown in Table 8. A detailed emission cross section spectrum around 2 μm is shown in Fig. 6, and the emission peak is around 2060 nm. Obviously, it is impossible to obtain σ_e for some other transitions, whose emission wavelength is beyond the absorption spectral range.

Table 8. Calculated results of emission cross section with the McCumber law.

Transition processes	$\lambda_{ap}/10^{-7}$ cm	Z_l/Z_u	E_0/cm^{-1}	$\sigma_e(\lambda_{ap})/10^{-21}$ cm^2
$^5I_7 \rightarrow {}^5I_8$	1948	0.81	5181	1.87
$^5I_6 \rightarrow {}^5I_8$	1150	0.86	8696	0.96
$^5I_5 \rightarrow {}^5I_8$	888	0.93	11236	0.34
$^5F_5 \rightarrow {}^5I_8$	640	0.86	15625	2.54
$^5S_2+{}^5F_4 \rightarrow {}^5I_8$	536	1.08	18478	2.18

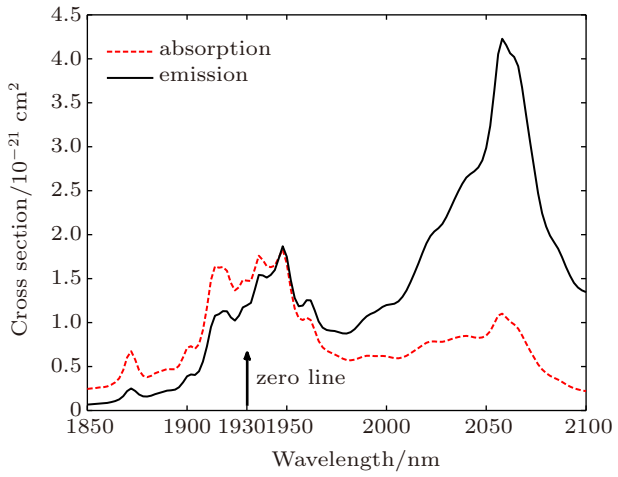


Fig. 6. Variations of the emission cross section with wavelength, calculated based on experimental absorption spectrum at room temperature.

3.4. Analyses of emission spectrum

The luminescence spectra at room temperature of 298 K are shown in Fig. 7, including the near-infrared range of 1850–2300 nm in Fig. 7(a), the mid-infrared range of 2775–3050 nm in Fig. 7(b) , and 3700–4400 nm in Fig. 7(c). Apparently, three characteristic emission peaks exist, and we list them in Table 9 together with their corresponding transition processes, and calculate the emission cross section at the wavelength of emission peak, λ_{ep}.

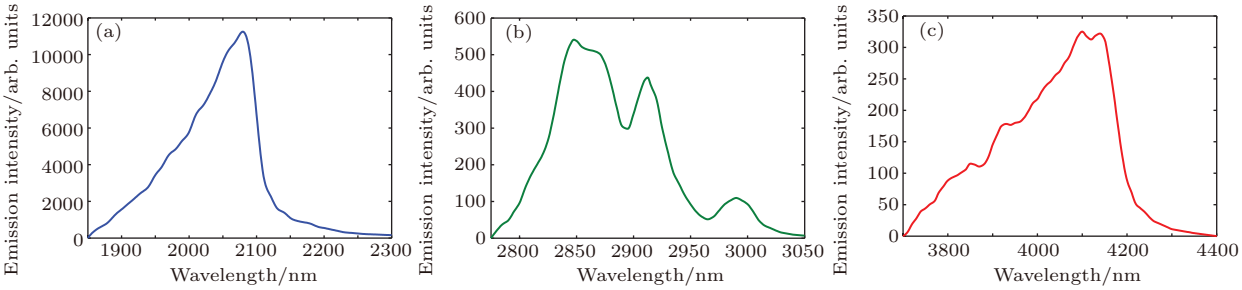


Fig. 7. Measured infrared luminescence spectra of 30 at.% Ho: BYF at room temperature. (a) Near-infrared spectrum around 2 μm, (b) mid-infrared spectrum around 3 μm, (c) mid-infrared spectrum around 4 μm.

Table 9. Calculated results of emission cross section with Füchtbauer–Ladenburg equation.

Transitions	τ_{rad}/ms	$\lambda_{ep}/10^{-7}$ cm	n/λ_{ep}	$\sigma_e(\lambda_{ep})/10^{-21}$ cm^2
$^5I_7 \rightarrow {}^5I_8$	22.03	2080	1.5164	3.82
$^5I_6 \rightarrow {}^5I_7$	169.78/57.27	2848	1.5161	2.82
$^5I_5 \rightarrow {}^5I_6$	512.82/136.05	4100	1.5159	4.37

According to the Füchtbauer–Ladenburg law[38] in Eq. (16), we calculate the emission cross section for radiation transition

$$\sigma_e(\lambda_e) = \frac{\eta\lambda_e^5}{8\pi n^2 c\tau_{rad}} \frac{I(\lambda_e)}{\int \lambda I(\lambda)\,d\lambda}, \tag{16}$$

where λ_e is the emission wavelength, $I(\lambda_e)$ the absolute value of emission intensity, and η the quantum emission efficiency. Herein we assume $\eta = 1$ without considering the non-radiative transitions.

The emission section at 2080 nm is about 2.09×10^{-21} cm^2 based on the reciprocity equation (15), a little smaller than that based on Füchtbauer–Ladenburg law, 3.82×10^{-21} cm^2. The main causes may be firstly that the vibronic interaction in Ho: BYF is prominent, resulting in non-reciprocity of σ_e and σ_a.[39] Secondly, the quantum emission efficiency should be less than 1 for the high dopant concentration. Meanwhile, the preliminarily calculated results for 2848 nm and 4100 nm are 2.82×10^{-21} cm^2 and 4.37×10^{-21} cm^2, respectively, with the emission spectra.

3.5. Preliminary laser emission

A mid-infrared Ho: BYF laser of plano–plano cavity is preliminarily built with our double lamp pumped Cr^{3+}: LiSAF laser, with a centarl wavelength of 889 nm. Cr^{3+}: LiSAF laser is operated with a repetition rate of 1 Hz and pulse duration of 50 μs, and its maximum output energy is 100 mJ. The size of Ho: BYF crystal is 3 mm × 3 mm × 2.8 mm. The transmittance of output mirror is 20% at 3.9 μm and a long-pass filter is used to inhibit the residual pump light. The output energy of 3.9 μm laser is about 5.61 mJ with an optical-to-optical conversion efficiency of 5.81%. Detailed output characteristics are shown in Fig. 8. The spectra are confirmed to be around 3886–3905 nm with a grating monochromator and the pulse width is about 35 μs. The output ability of our crystal is similar to the results given by Tabirian *et al.*[12] and Stutz *et al.*[16] when the pump energy is lower than 100 mJ. But Tabirian *et al.*[12] obtained a maximum energy of 30 mJ with a 1 cm in length, 20 at.% concentrated Ho:BYF crystal when the pump energy was increased to more than 320 mJ. And Stutz *et al.*[16] scaled up the output to 55 mJ with a 8 mm in length, 30 at.% concentrated Ho:BYF crystal when increasing the pump energy to more than 600 mJ. Considering the fact that the output of our Cr^{3+}:LiSAF laser is limited, we will investigate more detailed characteristics of the laser with our crystal in future studies.

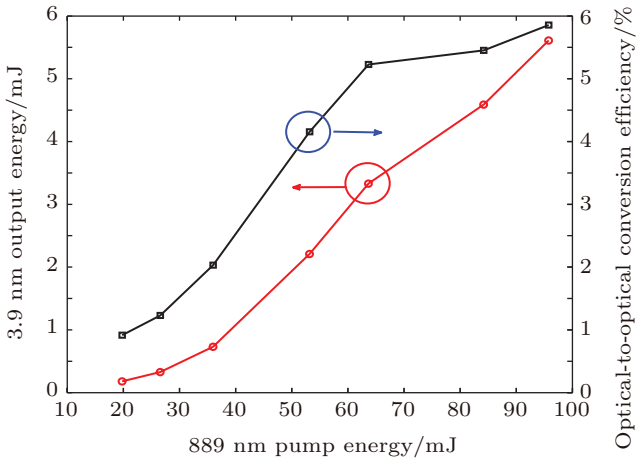


Fig. 8. Output characteristics of preliminary mid-infrared Ho: BYF laser pumped by 889 nm Cr^{3+}:LiSAF laser.

4. Conclusions

In summary, to our knowledge, it is the first time to systematically analyze the spectral properties of Ho: BYF crystal based on the standard Judd–Ofelt theory. With our 30 at.% Ho: BYF crystal, grown by the CZ method, the single-pass absorption coefficient, absorption cross section and J–O intensity parameters are determined with the measured absorption spectra. The optimized $\Omega_i\,(i=2,4,6)$ are $\Omega_2 = 6.74\times10^{-20}$ cm^2, $\Omega_4 = 1.20\times10^{-20}$ cm^2, and $\Omega_6 = 0.66\times10^{-20}$ cm^2. Furthermore, with the calculated Ω_i, we calculate the spontaneous emission probabilities, the fluorescence branching ratios, the radiation lifetimes and emission cross sections for a series of excited state manifolds, especially important for $^5I_5 \rightarrow {}^5I_6$ and $^5I_7 \rightarrow {}^5I_8$ transitions, whose emission wavelengths are about 4 μm and 2 μm, respectively. Then, we conduct a contrastive calculation of emission cross section with the McCumber law based on the absorption spectra and the Füchtbauer–Ladenburg law based on the measured luminescence spectra. The three important emission cross sections at wavelengths of 2080 nm, 2800 nm, and 4100 nm are 3.82×10^{-21}cm^2, 2.82×10^{-21} cm^2, and 4.37×10^{-21} cm^2, respectively. The results are basically satisfactory with our primary analysis. However, to obtain a more accurate calculation for Ho: BYF, a modified Judd–Ofelt model can be adopted.[38] Furthermore, detailed emission spectra for more transition processes can be measured to verify whether the values of Z_l/Z_u, and E_0 are reasonable. Finally, the preliminary mid-infrared laser emission experiment proves our crystal quality, and the 3.9 μm laser energy is obtained to be about 5.61 mJ.

References

[1] Jackson S D 2012 *Nat. Photonics* **6** 423
[2] Lippert E 2011 *Proc. SPIE* **8187** 81870F
[3] Serebryakov V A, Boiko E V, Petrishchev N N and Yan A V 2010 *J. Opt. Technol.* **77** 6
[4] Hemming A, Richards J, Bennetts S, Davidson A, Carmody N, Davies P, Corena L and Lancaster D 2010 *Opt. Commun.* **283** 4041
[5] Lippert E, Fonnum H, Arisholm G and Stenersen K 2010 *Opt. Exp.* **18** 26475
[6] Liu Q, Liu J H, Zhang Z L and Gong M L 2013 *Laser Phys. Lett.* **10** 075407
[7] Yao Y, Hoffman A J and Gmachl C F 2012 *Nat. Photonics* **6** 432
[8] Bowman S R, Shaw L B, Feldman B J and Ganem J 1996 *IEEE J. Quantum Elect.* **32** 646
[9] Adams J J, Bibeau C, Page R H, Krol D M, Furu L H and Payne S A 1999 *Opt. Lett.* **24** 1720
[10] Mirov S B, Fedorov V V, Martyshkin D V, Moskalev I S, Mirov M S and Gapontsev V P 2011 *Opt. Materials Exp.* **1** 898
[11] Tabirian A M, Buchter S C, Jenssen H P, Cassanho A and Hoffman H J 1999 *Conference on Lasers and Electro-Optics*, Baltimore, USA, p. CThJ2
[12] Tabirian A M, Jenssen H P and Cassanho A 2001 *Advanced Solid-State Lasers Congress*, Washington, USA, p. MC5
[13] Tsuboi T, Jang K H, Polosan S, Shimamura K, Bettinelli M and Seo H J 2011 *J. Lumin.* **131** 695
[14] Judd B R 1962 *Phys. Rev.* **127** 750
[15] Ofelt G S 1962 *J. Chem. Phys.* **37** 511
[16] Stutz R, Miller H and Dinndorf K 2004 *Proc. SPIE* **5332** 111
[17] Luo H, Qi L, Zhu S F, Guan Z. G, Zhang Z B, Zeng B and Guo C Y 2012 *J. Synthetic Crystals* **41** 1502
[18] Amaral J B, Couto dos Santos M A, Valerio M E G and Jackson R A 2005 *Appl. Phys. B-Lasers O.* **81** 841
[19] Kaminskii A A, Sarkisov S E, Below F and Eichler H J 1990 *Opt. Quant. Electron.* **22** S95
[20] Guilbert L H, Gesland J Y, Bulou A and Retoux R 1993 *Mater. Res. Bull.* **28** 923
[21] Axe Jr J D 1963 *J. Chem. Phys.* **39** 1154
[22] Fowler W B and Dexter D L 1962 *Phys. Rev.* **128** 2154
[23] Walsh B M, Norman P B and Baldassare D B 1998 *J. Appl. Phys.* **83** 2772
[24] Weber M J 1995 *CRC Handbook of Laser Science and Technology*, 1st edn. (Boca Raton: CRC Press) pp. 600–605
[25] Carnall W T, Fields P R and Rajna K 1968 *J. Chem. Phys.* **49** 4424
[26] Carnall W T, Crosswhite H and Crosswhite H M 1978 (personal communication)
[27] Bullock S R, Reddy B R and Venkateswarlu P 1997 *J. Opt. Soc. Am. B* **14** 553
[28] Shojiya M and Kawamoto Y 2001 *J. Appl. Phys.* **89** 4944
[29] Walsh B M, Grew G W and Barnes N P 2006 *J. Phys. Chem. Solids* **67** 1567
[30] Sani E, Toncelli A and Tonelli M 2006 *J. Phys-Condens. Mat.* **18** 2057
[31] Gheorghe C, Lupei A, Lupei V, Gheorghe L and Ikesue A 2009 *J. Appl. Phys.* **105** 123110
[32] Peng J T, Xia H P, Wang P Y, Hu H Y and Tang L 2013 *Chinese J. Lumin.* **34** 702
[33] Jorgensen C K and Reisfeld R 1983 *J. Less-Common. Met.* **93** 107
[34] Peacock R D 1975 *Struct. Bond.* **22** 83
[35] Krupke W F 1966 *Phys. Rev.* **145** 325
[36] McCumber D E 1964 *Phys. Rev. A* **136** 954
[37] Payne S A, Chase L L, Smith L K, Kway W L and Krupke W F 1992 *IEEE J. Quantum Elect.* **28** 2619
[38] Aull B F and Jenssen H P 1982 *IEEE J. Quantum Elect.* **18** 925
[39] Goldner P 1996 *J. Appl. Phys.* **79** 7972